CHIN. PHYS. LETT. Vol. 37, No. 12 (2020) 124202

Hermite Non-Uniformly Correlated Array Beams and Its Propagation Properties

Xue-Chun Zhao(赵雪纯)[1], Lei Zhang(张磊)[1], Rong Lin(林蓉)[1,2], Shu-Qin Lin(蔺淑琴)[1], Xin-Lei Zhu(朱新蕾)[3], Yang-Jian Cai(蔡阳健)[1,3*], and Jia-Yi Yu(余佳益)[1*]

[1]*Shandong Provincial Engineering and Technical Center of Light Manipulations & Shandong Provincial Key Laboratory of Optics and Photonic Device, School of Physics and Electronics, Shandong Normal University, Jinan 250014, China*
[2]*College of Physics and Electronic Engineering, Heze University, Heze 274015, China*
[3]*School of Physical Science and Technology, Soochow University, Suzhou 215006, China*

(Received 28 September 2020; accepted 4 November 2020; published online 8 December 2020)

We study the evolution of spectral intensity and degree of coherence of a new class of partially coherent beams, Hermite non-uniformly correlated array beams, in free space and in turbulence, based on the extended Huygens–Fresnel integral. Such beams possess controllable rectangular grid distributions due to multi-self-focusing propagation property. Furthermore, it is demonstrated that adjusting the initial beam parameters, mode order, shift parameters, array parameters and correlation width plays a role in resisting intensity and degree of coherence degradation effects of the turbulence.

PACS: 42.25.−p, 42.25.Kb, 42.25.Bs, 42.25.Dd DOI: 10.1088/0256-307X/37/12/124202

Laser has certain advantages in many aspects such as free space optical (FSO) communication, lidar and remote sensing, due to directionality, brightness, monochromaticity and coherence properties of laser. However, in these applications, laser takes atmosphere as the information transmission channel, and over significant propagation distances, the laser beams will experience random wavefront fluctuations due to atmospheric turbulence, leading to some negative effects. This increases the signal data error rate at the receiving end, limiting the performance of the communication systems.[1] Therefore, it is of great scientific and practical importance to study how to reduce the negative effects of atmospheric turbulence on laser beams.

Heretofore, many papers have studied strategies to reduce the negative effects in turbulent atmosphere by adjusting different degree of freedom of laser beams. It is now well-known that coherence adjusting is one of the valid strategies to improve the performance of laser beams in turbulence[2] and it is also a strategy for encoding information into correlation structure for transmission.[3] In particular, laser beams with low spatial coherence, labeled partially coherent beams (PCBs),[4] have lower turbulence-induced negative effects than their fully coherent counterparts.[1,2] The physical mechanism for the resistance of PCBs to turbulence can be explained from the point of view of the coherent mode representation, which indicates that light is sent simultaneously through distinct non-interfering channels.[5,6] Spatially variant correlation structure, non-uniformly correlated (NUC) beams,[7−10] is a broad and extremely important class derived from the formalism by Gori *et al.*[10] NUC beams display some extraordinary properties, such as self-focusing and self-shifting and it was shown that such beams can have, under certain circumstances, not only lower scintillation but higher intensity than Gaussian Schell-model (GSM) beams in turbulence.[11,12] Thus, PCBs with non-uniformly correlation structure achieve both high intensity and low scintillation, it is desirable especially when laser beams are used in FSO communications.[8,11−13]

On the other hand, the array beams were widely studied due to its widely applications. Increasing resistance to turbulence of laser beams by array distribution design is one of the important applications. Up to now, many studies have shown that beam arrays are usually superior to a single beam for reducing the negative effects of turbulence.[14] Lots of papers introduced a variety of partially coherent array beams with special beam profile,[15] phase,[16,17] polarization[18] and correlation structure.[19] However, the vast majority of related works focus on the array beams with uniform source. The study of partially coherent array beams with non-uniformly correlation structure has not been reported yet.

The spatial coherence properties of PCBs in scalar case are expressed by the cross-spectral density (CSD) function in space-frequency domain. To be a mathematically genuine and physically realizable correlation

Supported by the National Key Research and Development Program of China (Grant No. 2019YFA0705000), the National Natural Science Foundation of China (Grant Nos. 91750201, 11525418, 11947240, 11974218, 12004218, and 11904087), the Local Science and Technology Development Project of the Central Government (Grant No. YDZX20203700001766), and Innovation Group of Jinan (Grant No. 2018GXRC010).
*Corresponding authors. Email: yangjiancai@suda.edu.cn; jiayiyu0528@sdnu.edu.cn
© 2020 Chinese Physical Society and IOP Publishing Ltd

function of PCBs, the CSD function needs to satisfy the non-negative definiteness condition[10]

$$W(\boldsymbol{r}_1,\boldsymbol{r}_2)=\int I(\boldsymbol{v})H_0^*(\boldsymbol{r}_1,\boldsymbol{v})H_0(\boldsymbol{r}_2,\boldsymbol{v})d^2\boldsymbol{v}, \quad (1)$$

where $I(\boldsymbol{v})$ is a non-negative function and $H_0(\boldsymbol{r},\boldsymbol{v})$ denotes an arbitrary kernel.

Next, we devise $H_0(\boldsymbol{r},\boldsymbol{v})$ as

$$H_0(\boldsymbol{r},\boldsymbol{v})=\exp(-\boldsymbol{r}^2/w_0^2)\sum_{M=-p}^{p}\sum_{N=-q}^{q}\cdot\exp[-ik\Re(\boldsymbol{r},M,N)\cdot\boldsymbol{v}], \quad (2)$$

where w_0 is the beam width, $\Re(\boldsymbol{r},M,N)$ is a real vector function, $k=2\pi/\lambda$ denotes the wavenumber with the wavelength λ, and the array parameters p and q are for x and y directions.

According to Eqs. (1) and (2), we derive the CSD function expressed as

$$W(\boldsymbol{r}_1,\boldsymbol{r}_2)=\exp[-(\boldsymbol{r}_1^2+\boldsymbol{r}_2^2)/w_0^2]\mu(\boldsymbol{r}_1,\boldsymbol{r}_2), \quad (3)$$

where $\mu(\boldsymbol{r}_1,\boldsymbol{r}_2)$ is the degree of coherence (DOC), which is the Fourier transform of function $I(\boldsymbol{v})$, i.e.,

$$\mu(\boldsymbol{r}_1,\boldsymbol{r}_2)=\sum_{M=-p}^{p}\sum_{N=-q}^{q}\tilde{I}[\Re(\boldsymbol{r}_2,M,N)-\Re(\boldsymbol{r}_1,M,N)]. \quad (4)$$

From Eq. (4), we find that the DOC of PCBs exhibits array structure and depends on the form of $I(\boldsymbol{v})$ and $\Re(\boldsymbol{r},M,N)$.

We introduce a generalized array set of higher-order sources with

$$I(\boldsymbol{v})=(a^2\pi)^{-1}(4v_xv_y/a^2)^{2\,m}\exp[-(v_x^2+v_y^2)/a^2], \quad (5)$$

$$\Re(\boldsymbol{r},M,N)=(x-Mx_0)^2\boldsymbol{i}+(y-Ny_0)^2\boldsymbol{j}, \quad (6)$$

where a is positive real constant, m is the mode order, x_0 and y_0 are the shift parameters in x and y directions.

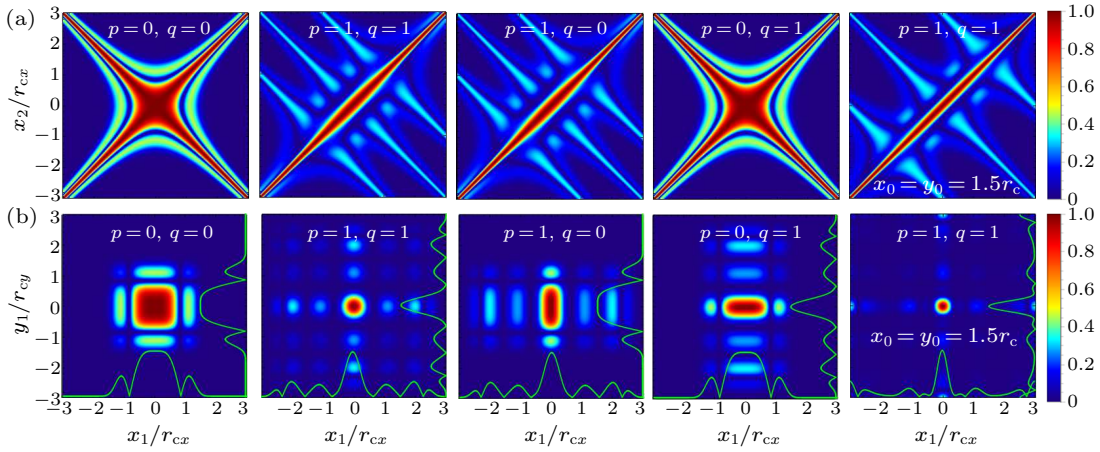

Fig. 1. Density plot of the absolute value of the DOC of the proposed beams for different array parameters with $m=1$ and $x_0=y_0=r_c$ or $x_0=y_0=1.5r_c$ (a) in the x_1–x_2 plane and (b) in the x_1–y_1 plane.

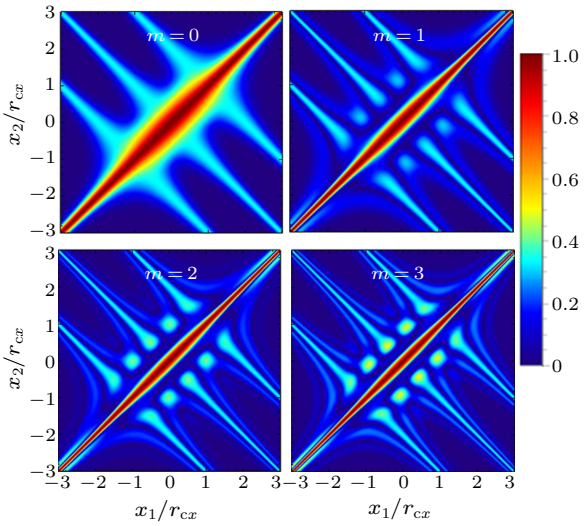

Fig. 2. Density plot of the absolute value of the DOC of the proposed beams for different mode orders with $p=q=1$ and $x_0=y_0=r_c$ in the x_1–x_2 plane.

Substituting Eqs. (2), (5) and (6) into Eq. (1), we derive readily the CSD expression of the generated PCBs,

$$W(\boldsymbol{r}_1,\boldsymbol{r}_2)=\sum_{M=-p}^{p}\sum_{N=-q}^{q}G_0^2\exp\left(-\frac{\boldsymbol{r}_1^2+\boldsymbol{r}_2^2}{w_0^2}\right)\cdot\exp\left[-\frac{(X^2-Y^2)}{r_c^4}\right]H_{2m}\left(\frac{X}{r_c^2}\right)H_{2m}\left(\frac{Y}{r_c^2}\right), \quad (7)$$

with $X=[(x_1-Mx_0)^2-(x_2-Mx_0)^2]$ and $Y=[(y_1-Ny_0)^2-(y_2-Ny_0)^2]$; $r_c=(2/ka)^{1/2}$ is the correlation width, $G_0=1/H_{2m}(0)$ with $H_{2m}(\cdots)$ denotes the Hermite polynomials of order $2m$.

Figure 1 shows the two-dimension density plot of the absolute value of the DOC of the proposed beams for different values of p and q in the source plane. We confirm from Fig. 1(a) that the high-coherence area of the proposed beams is confined to along one diago-

nal (around $x_1 = x_2$, let us define it as R-diagonal), and it is also confined to along and parallel to another diagonal (around $x_1 = -x_2$, let us define it as L-diagonal). Furthermore, the number of the high-coherence stripes in L-diagonal direction is dependent on the value of array parameters and the spacing between the high-coherence stripes is dependent on the values of the shift parameters x_0 and y_0. Figure 1(b) shows the rectangular array distribution of the DOC of the proposed beams in the x_1–y_1 plane. The number of side lobes in x and y directions increases as the values of the array parameters p and q increase.

Figure 2 shows the distribution of the absolute value of the DOC of the proposed beams for different mode orders. We find that the number of side lobes around the high-coherence area increases as the value of the mode order m increases. Considering the novel distribution of the DOC from Figs. 1 and 2, we therefore have a class of Hermite non-uniformly correlated array (HNUCA) beams with distinct DOC.

Under the paraxial approximation, the CSD of HNUCA beams in an arbitrary plane of propagation in random medium can be studied with the help of the generalized Huygens–Fresnel principle,[20]

$$\begin{aligned} &W(\boldsymbol{\rho}_1, \boldsymbol{\rho}_2, z) \\ &= \Big(\frac{k}{2\pi z}\Big)^2 \int\int_{-\infty}^{\infty} W_0(\boldsymbol{r}_1, \boldsymbol{r}_2) \\ &\quad \cdot \exp\Big[-\frac{ik}{2z}(\boldsymbol{r}_1 - \boldsymbol{\rho}_1)^2 + \frac{ik}{2z}(\boldsymbol{r}_2 - \boldsymbol{\rho}_2)^2\Big] \\ &\quad \times \langle \exp[\Psi(\boldsymbol{r}_1, \boldsymbol{\rho}_1) + \Psi^*(\boldsymbol{r}_2, \boldsymbol{\rho}_2)]\rangle d^2\boldsymbol{r}_1 d^2\boldsymbol{r}_2, \end{aligned} \tag{8}$$

where $\boldsymbol{\rho}_1$ and $\boldsymbol{\rho}_2$ represent two arbitrary position vectors in the target plane, z is the propagation distance, $W_0(\boldsymbol{r}_1, \boldsymbol{r}_2)$ denotes the CSD of PCBs in the source plane, and $\Psi(\boldsymbol{r}, \rho)$ denotes the complex phase perturbation due to the refractive-index fluctuations of the random medium between the source plane and receiving plane. The ensemble average term in the above equation can be approximated to

$$\begin{aligned} &\langle \exp[\Psi(\boldsymbol{r}_1, \boldsymbol{\rho}_1) + \Psi^*(\boldsymbol{r}_2, \boldsymbol{\rho}_2)]\rangle \\ &= \exp\Big\{-\frac{\pi^2 k^2 z}{3}[(\boldsymbol{\rho}_1 - \boldsymbol{\rho}_2)^2 + (\boldsymbol{\rho}_1 - \boldsymbol{\rho}_2)\cdot(\boldsymbol{r}_1 - \boldsymbol{r}_2) \\ &\quad + (\boldsymbol{r}_1 - \boldsymbol{r}_2)^2]\int_0^{\infty} \kappa^3 \Phi_n(\kappa) d^2\kappa\Big\}, \end{aligned} \tag{9}$$

with κ being the magnitude of the spatial wave number and $\Phi_n(\kappa)$ the spatial power spectrum of the refractive-index fluctuations of the turbulent medium. The model of the power spectrum we chose is built by the van Karman power spectrum[21]

$$\begin{aligned} \Phi_n(\kappa) = A(\alpha) C_n^2 (\kappa^2 + \kappa_0^2)^{-\alpha/2} \exp(-\kappa^2/\kappa_m^2), \\ 0 \leqslant \kappa \leqslant \infty, \quad 3 < \alpha < 4. \end{aligned} \tag{10}$$

where $A(\alpha) = \Gamma(\alpha - 1)\cos(\alpha\pi/2)/(4\pi^2)$ with $\Gamma(\cdots)$ represents the incomplete Gamma function; C_n^2 is a generalized refractive-index structure parameter in units of $m^{3-\alpha}$; $\kappa_0 = 2\pi/L_0$ and $\kappa_m = c(\alpha)/l_0$ with $c(\alpha) = [2\pi A(\alpha)\Gamma(5/2 - \alpha/2)/3]^{1/(\alpha-5)}$, L_0 and l_0 are the outer and inner scales of turbulence, respectively.

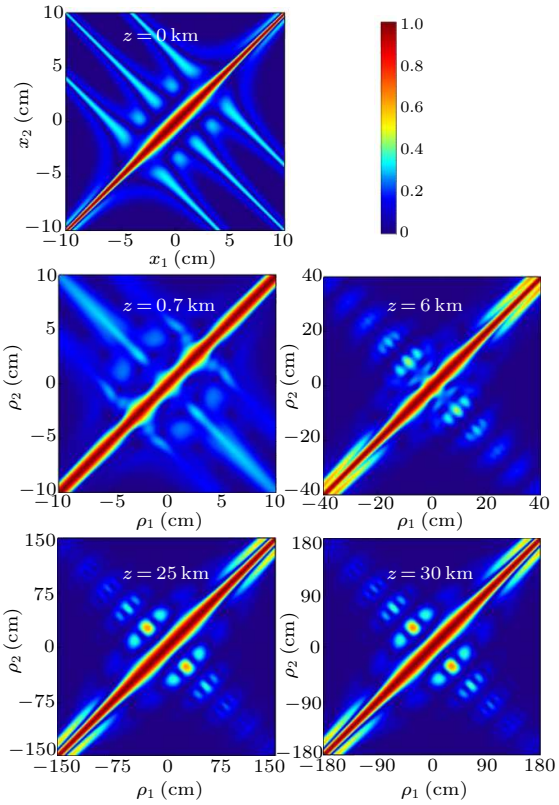

Fig. 3. Density plot of the absolute value of the spectral DOC of HNUCA beams with $m = 1$, $p = q = 1$, $r_c = 3$ cm and $x_0 = y_0 = 3$ cm for different distances in free space.

Substituting Eq. (1) into Eq. (8), after interchanging the orders of the integrals, we obtain

$$W(\boldsymbol{\rho}_1, \boldsymbol{\rho}_2, z) = \int I(\boldsymbol{v}) P(\boldsymbol{\rho}_1, \boldsymbol{\rho}_2, \boldsymbol{v}, z) d^2\boldsymbol{v}, \tag{11}$$

with

$$\begin{aligned} &P(\boldsymbol{\rho}_1, \boldsymbol{\rho}_2, \boldsymbol{v}, z) \\ &= \frac{w_0^2}{2w_{zx}w_{zy}} \exp\Big[-\frac{ik}{2z}(\boldsymbol{\rho}_1^2 - \boldsymbol{\rho}_2^2)\Big] \\ &\quad \cdot \exp\Big[-\Big(\frac{k^2 w_0^2}{8z^2} + \frac{1}{3}\pi^2 k^2 z T\Big)(\boldsymbol{\rho}_1 - \boldsymbol{\rho}_2)^2\Big] \\ &\quad \cdot \sum_{M=-p}^{p} \exp\Big\{-\frac{1}{w_{zx}^2}\Big| - i\Big[\frac{w_0^2 k}{4z}(1 - 2v_x z) - \frac{1}{3}\pi^2 k z^2 T\Big] \\ &\quad \cdot (\rho_{1x} - \rho_{2x}) + \frac{1}{2}(\rho_{1x} + \rho_{2x}) - 2v_x z M x_0\Big|^2\Big\} \\ &\quad \cdot \sum_{N=-q}^{q} \exp\Big\{-\frac{1}{w_{zy}^2}\Big| - i\Big[\frac{w_0^2 k}{4z}(1 - 2v_y z) - \frac{1}{3}\pi^2 k z^2 T\Big] \\ &\quad \cdot (\rho_{1y} - \rho_{2y}) + \frac{1}{2}(\rho_{1y} + \rho_{2y}) - 2v_y z N y_0\Big|^2\Big\}, \end{aligned} \tag{12}$$

where

$$w_{z\xi} = \left[\frac{w_0^2}{2}(1-2v_\xi z)^2 + \left(\frac{\sqrt{2}z}{kw_0}\right)^2 + \frac{4\pi^2 z^3}{3}T\right]^{1/2}, \quad \xi = x, y. \tag{13}$$

The spectral intensity and the DOC of HNUCA beams, in the target plane, are defined as

$$S(\boldsymbol{\rho}, z) = W(\boldsymbol{\rho}, \boldsymbol{\rho}, z), \tag{14}$$

$$\mu(\boldsymbol{\rho}_1, \boldsymbol{\rho}_2, z) = \frac{W(\boldsymbol{\rho}_1, \boldsymbol{\rho}_2, z)}{\sqrt{W(\boldsymbol{\rho}_1, \boldsymbol{\rho}_1, z)W(\boldsymbol{\rho}_2, \boldsymbol{\rho}_2, z)}}. \tag{15}$$

It is worth mentioning that we can obtain the expression of CSD of HNUCA beams after propagation in free space just by setting $C_n^2 = 0$, as well as the spectral intensity and DOC.

Using the expressions derived above, we study the evolution of the spectral DOC and intensity of HNUCA beams in free space and turbulent atmosphere. In the following examples, the relevant initial parameters of HNUCA beams and turbulence are set as $\lambda = 632.8\,\text{nm}$, $w_0 = 5\,\text{cm}$, $L_0 = 1\,\text{m}$, $l_0 = 1\,\text{mm}$ and $C_n^2 = 10^{-15}\,\text{m}^{-2/3}$. For convenience, the wavelength of the common HeNe-type laser diodes was used. The results presented here are qualitatively similar in optical communication wavelengths.

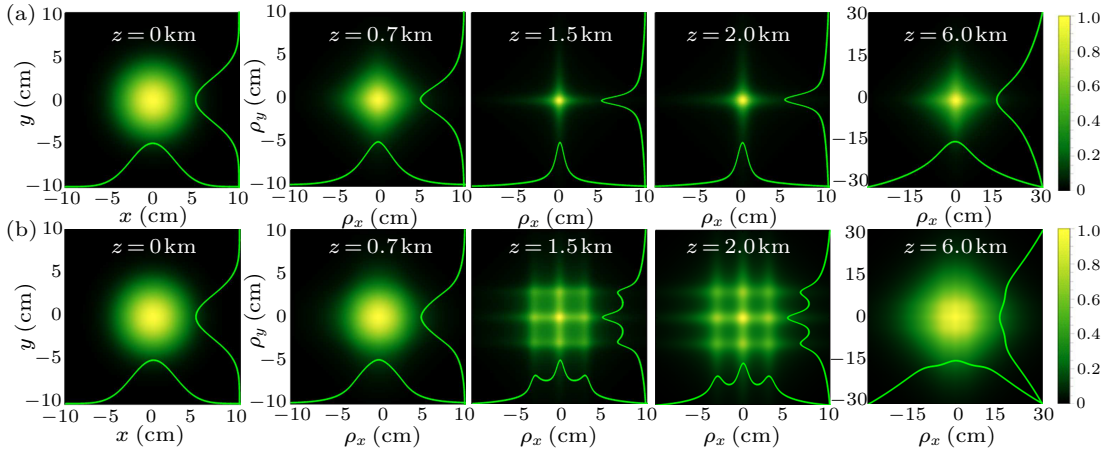

Fig. 4. The spectral intensity of HNUCA beams with $m = 1$, $r_c = 3\,\text{cm}$, $x_0 = y_0 = 3\,\text{cm}$: (a) $p = q = 0$, (b) $p = q = 1$, for different distances in free space.

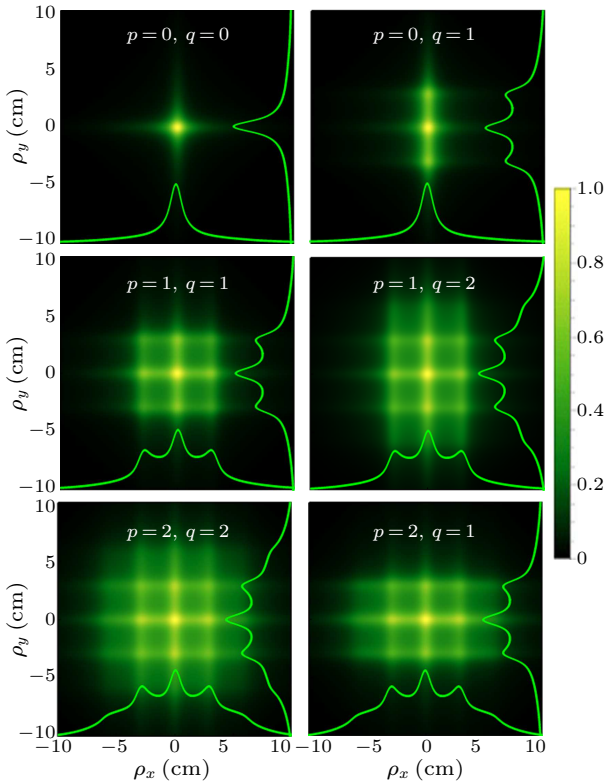

Fig. 5. Distributions of the spectral intensity of HNUCA beams with $m = 1$, $r_c = 3\,\text{cm}$ and $x_0 = y_0 = 3\,\text{cm}$ for different array parameters at focal distances.

Figure 3 shows the density plot of the absolute value of the DOC of HNUCA beams propagation in free space and the coherence of such beams displays striking effects. We confirm that the high-coherence area of HNUCA beams is always confined to along R-diagonal on propagation. The coverage of the high-coherence stripes along L-diagonal area is broken down and reorganized, when such beams propagate in free space.

Figure 4 shows the normalized intensity distribution of HNUCA beams propagation in free space for different values of array parameters. Figure 4(a) shows the evolution of spectral intensity of such beams with $p = q = 0$, i.e., rectangular Hermite non-uniformly correlated beams. One observes that such beams possess self-focusing property, which has been reported in Ref. [8]. One confirms from Fig. 4(b) that HNUCA beams with $p = q = 1$ display multi-self-focusing and self-combining properties on propagation, i.e., the initial single beam spot evolves into rectangular grid distribution (multiple beam spots) over short ranges, while in long ranges, the beam spots combine into one beam spot again on propagation in free space, which are totally different from those of single form rectangular Hermite non-uniformly correlated beams.[8]

In order to much more clearly show the relationship between the number and distribution of the multi high-light cores (multi-focus) and the values of p and q. Figure 5 shows the spectral intensity distribution at focal distance for different values of p and q. We find the number of foci in x and y directions is dependent on the values of p and q, respectively. The initial beam single spot evolves into $(2p+1)\times(2q+1)$ beam spots on propagation. Thus, we can modulate the distribution of the intensity at focal distance conveniently by adjusting the values of p and q. The extraordinary propagation property suggests that HNUCA beams may be useful in relevant applications, e.g., the obtained intensity array distribution in the focal plane can be used to simultaneously trap multiple particles whose refractive indices are larger than that of the ambient.

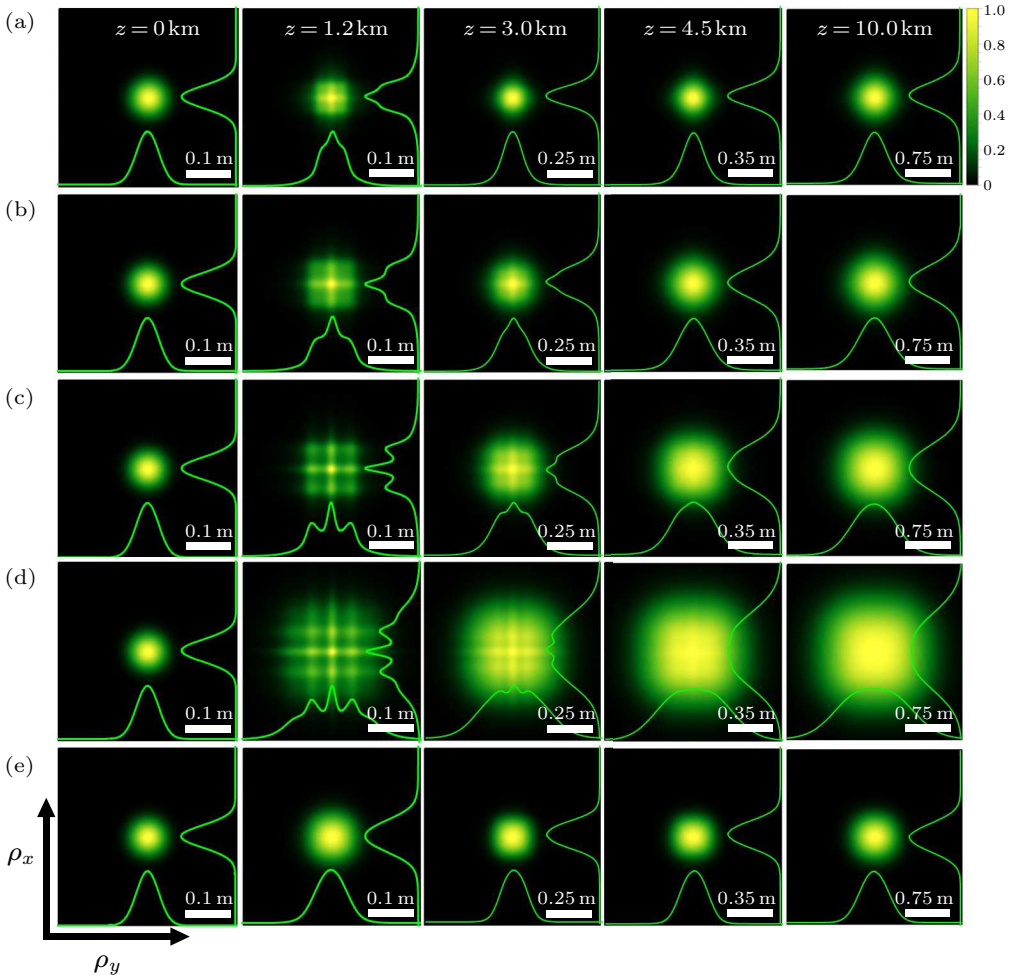

Fig. 6. The evolution of spectral intensity of HNUCA beams with (a) $m=1$, $p=q=1$, $r_c=3$ cm and $x_0=y_0=3$ cm; (b) $m=1$, $p=q=1$, $r_c=3$ cm and $x_0=y_0=5$ cm; (c) $m=2$, $p=q=1$, $r_c=3$ cm and $x_0=y_0=5$ cm; (d) $m=2$, $p=q=2$, $r_c=3$ cm and $x_0=y_0=5$ cm; (e) $m=2$, $p=q=2$, $r_c=5$ cm and $x_0=y_0=5$ cm in turbulence.

Figure 6 shows the evolution of spectral intensity of HNUCA beams for different initial beam parameters propagation in turbulence. One finds from Fig. 6 that the HNUCA beams with different initial beam parameters, in the source plane, all have a Gaussian beam profile and such beams display multi-self-focusing property in short propagation distance in turbulence. This propagation property is similar to that in free space as shown above. While at long propagation distance, the beam profile of HNUCA beams convert from array distribution to Gaussian distribution. This phenomenon can be explained by the fact that the influence of turbulence can be neglected and the free-space diffraction plays a major role at short propagation distance, thus the propagation property of HNUCA beams in turbulence is similar to those in free space. With the further increase of distance, the influence of turbulence accumulates and plays a dominant role gradually, and the array beam spots evolve into one beam spot again at long propagation distance due to the isotropic influence of turbulence.

In the following, we will detailedly discuss the effects of different initial beam parameters on the turbulence resistance of HNUCA beams from the aspect of

beam spots evolution. Comparing Figs. 6(a) and 6(b), we find that the conversion from the array distribution to Gaussian distribution becomes slower as the shift parameters increase, which means that HNUCA beams with large shift parameters are less affected by turbulence. Comparing with Figs. 6(b) and 6(c), one can confirm that for different mode orders, HNUCA beams evolve in a nontrivial manner, manifesting different split space of these focused beam spots. HNUCA beams with large mode order can maintain its array beam distribution over a longer propagation distance, which means that HNUCA beams with large mode order are less affected by turbulence or exhibit better turbulence resistance. One can further confirm from Figs. 6(c) and 6(d) that large array parameters cause such beams to exhibit more beam spots in array beam distribution and to show much better turbulence resistance from the aspect of the beam distribution degenerate to Gaussian distribution. Figures 6(d) and 6(e) show that the effect of correlation width is significant, HNUCA beams with low coherence display well multi-self-focusing property and maintain multi-focus state over a longer propagation distance. To sum up, HNUCA beams exhibit better turbulence resistance with large beam shift parameters, mode order, array parameters and/or low coherence from the aspect of beam spot conversion from the array distribution to Gaussian distribution.

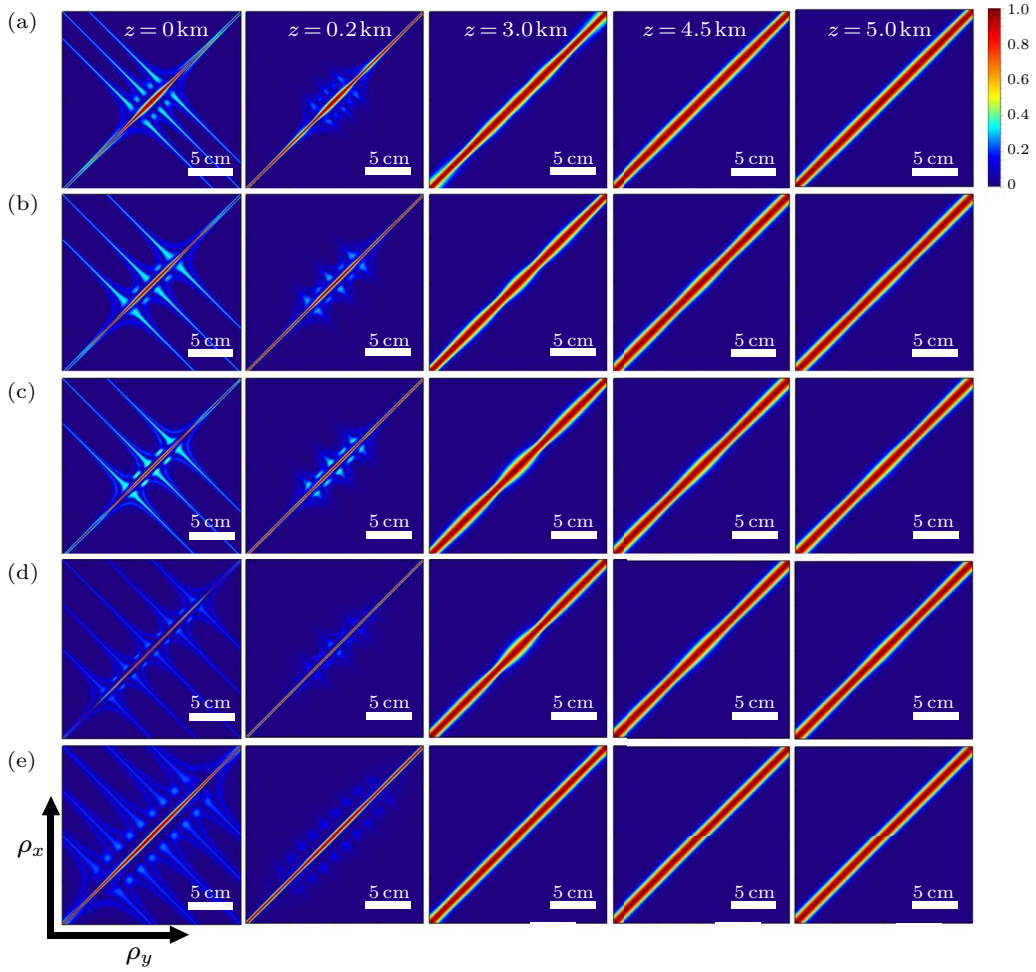

Fig. 7. The evolution of the absolute value of the DOC of HNUCA beams for different initial beam parameters (the parameters are the same as those in Fig. 6) in turbulence.

Figure 7 shows the evolution of the absolute value of the DOC of HNUCA beams for different values of the initial beam parameters in turbulence. Compared to Fig. 3, it shows that the high-coherence around L-diagonal is getting weaker after such beam propagation in turbulence. As the propagation distance increases further, the distribution of the CSD becomes spatially quasi-homogeneous, nearly constant along the R-diagonal lines. Furthermore, one confirms that the coverage of the high-coherence area of such beams reduces more slowly with larger beam shift parameters in comparison of Figs. 7(a) and 7(b). This means that HNUCA beams with large beam shift parameters can more easily keep the initial DOC distribution in turbulence, i.e., it has better turbulence resistance. We find from Figs. 7(b) and 7(c) that HNUCA beams with large mode order exhibit better turbulence resistance also from the aspect of degeneration of the

DOC. Similarly, we say the evolution properties of the DOC are closely related to the values of array parameters and correlation width, HNUCA beams with low coherence are less affected by turbulence from the perspective of the conversion of the CSD from spatially non-homogeneous to spatially quasi-homogeneous, in comparison of Figs. 7(d) and 7(e).

We have learned the propagation properties of HNUCA beams in free space and in turbulence, and found that the propagation properties of such beams are quite different from those of NUC beams with conventional single form correlation structures. Our results show that we can adjust the array parameters of HNUCA beams to control the rectangular grid distribution in focal distance. Furthermore, HNUCA beams with large shift parameters, mode order, array parameters and/or low coherence are less affected by turbulence than such beams with small shift parameters, mode order, array parameters and/or high coherence.

It is worthwhile to say a few words about the physics mechanism that leads HNUCA beams to have their unusual properties. Viewing Eq. (1) as an integral over coherent modes of the beam, Eq. (2) shows that HNUCA beams are combined with different modes that have different shift parameters, and each of the modes possesses a quadratic phase factor, $\exp[-ik\Re(\boldsymbol{r}, M, N) \cdot \boldsymbol{v}]$, which causes them to individually converge at different focal distances given by the expression $z = 1/2v$. Thus, HNUCA beams exhibit array distribution at focal distances, then each mode defocused after focal distance and gradually they combine into one beam spot.

We have also seen that HNUCA beams with large shift parameters, mode order, array parameters and/or low coherence exhibit well turbulence resistance. For the beams with higher mode order and lower coherence, they will focus at closer points than lower mode order modes and higher coherence, which indicates that they spreads more rapidly over long propagation distances. For the beams with large shift parameters and array parameters, they will spread much more rapidly than those with small shift parameters and array parameters. Both the cases make the beam components propagate at larger angles with respect to the beam axis, the turbulence is less likely to scatter them back along the axis. This explains why HNUCA beams with large shift parameters, mode order, array parameters and/or low coherence exhibit well turbulence resistance.

Our results show that the beams with an array distribution correlation structure display a controlled beam array shape and more resistance to turbulence, which can be tailored for the multiple particles trapping application needs. This flexibility of adjusting initial beam parameters can be used to improve the characteristics of beams in FSO communications.

References

[1] Gbur G 2014 *J. Opt. Soc. Am. A* **31** 2038
[2] Wang F, Liu X and Cai Y 2015 *Prog. Electromagn. Res.* **150** 123
[3] Chen Y, Ponomarenko S A and Cai Y 2016 *Appl. Phys. Lett.* **109** 061107
[4] Cai Y, Chen Y, Yu J, Liu X and Liu L 2017 *Prog. Opt.* **62** 157
[5] Gbur G and Wolf E 2002 *J. Opt. Soc. Am. A* **19** 1592
[6] Shirai T, Dogariu A and Wolf E 2003 *J. Opt. Soc. Am. A* **20** 1094
[7] Lajunen H and Saastamoinen T 2013 *Opt. Express* **21** 190
[8] Yu J, Cai Y and Gbur G 2018 *Opt. Express* **26** 27894
[9] Yu J, Zhu X, Lin S, Wang F, Gbur G and Cai Y 2020 *Opt. Lett.* **45** 3824
[10] Gori F and Santarsiero M 2007 *Opt. Lett.* **32** 3531
[11] Gu Y and Gbur G 2013 *Opt. Lett.* **38** 1395
[12] Yu J, Wang F, Liu L, Cai Y and Gbur G 2018 *Opt. Express* **26** 16333
[13] Lin S, Wang C, Zhu X, Lin R, Wang F, Gbur G, Cai Y and Yu J 2020 *Opt. Express* **28** 27238
[14] Cai Y, Chen Y, Eyyuboglu H T and Baykal Y 2007 *Appl. Phys. B* **88** 467
[15] Zhou X, Zhou Z, Tian P and Yuan X 2019 *Appl. Opt.* **58** 9443
[16] Singh R K, Sharma A M and Senthilkumaran P 2015 *Opt. Lett.* **40** 2751
[17] Wan L and Zhao D 2018 *Opt. Lett.* **43** 3554
[18] Mu T, Chen Z, Pacheco S, Wu R, Zhang C and Liang R 2016 *Opt. Lett.* **41** 261
[19] Liang C, Zhu X, Mi C, Peng X, Wang F, Cai Y and Ponomarenko S A 2018 *Opt. Lett.* **43** 3188
[20] Andrews L C and Phillips R L 2005 *Laser Beam Propagation through Random Media* 2nd edn (Bellinghan: SPIE)
[21] Toselli I, Andrews L C, Phillips R L and F V 2008 *Opt. Eng.* **47** 026003